Proceedings of 20th International Congress on Acoustics, ICA 2010

23-27 August 2010, Sydney, Australia

Theory and Phenomenology of the Acoustic Vector Field

Kevin B. Smith

Dept of Physics, Naval Postgraduate School, Monterey, CA, USA

PACS: 43.10.Df, 43.20.Bi, 43.30.Bp, 43.30.Pc

ABSTRACT

In this paper, a review of several features of the acoustic vector field will be presented. The theoretical foundation for the acoustic energy flow will be used to describe the concepts of the active and reactive components of the complex acoustic intensity field. Recently established phenomenology associated with the flow of acoustic intensity near planar boundaries via the visualization of streamlines will also be discussed. Features of the complex field scattered from simple objects will be presented, along with phenomenology found in multipath environments such as channels and waveguides. Methods for validating vector field extensions of existing numerical models in the field of underwater acoustics are defined, and some specific examples of the properties of the complex field in ocean environments is provided. Methods for extracting information about the seafloor (e.g., geoacoustic inversion) are also described. Finally, a brief overview of common beamforming techniques is presented. [Work supported by the US Office of Naval Research, Code 322OA.]

BACKGROUND

For many years, the acoustics community has relied solely upon measurements of the pressure field to determine acoustic intensity, i.e. the acoustic energy flux density. In the presence of plane waves, such knowledge of the pressure field was sufficient to determine the magnitude of the acoustic intensity. However, in many cases, additional information is required to formally define the total acoustic intensity. Furthermore, acoustic intensity is fundamentally a vector quantity, providing information on the directional flow of acoustic energy. Studies of the full vector acoustic field then require the use of directional sensors.

Some of the earliest work in the field of underwater acoustics to study vector intensity was performed by D'Spain,[1, 2] who utilized directional Swallow floats to investigate the directional nature of ultra-low frequency (infrasonic) noise in the Pacific Ocean, just west of San Diego. This also helped establish the formal description of the complex vector intensity.

Specifically, we apply a conservation of energy argument to the linear acoustic equation in a lossless fluid medium to obtain

$$\frac{\partial}{\partial t}\left(\frac{1}{2}\rho u^2+\frac{1}{2}\frac{p^2}{\rho c^2}\right)+\nabla\bullet\left(p\vec{u}^*\right)=0\ , \tag{1}$$

where the velocity associated wth the displacement of the fluid medium is related to the pressure by

$$\vec{u}=\frac{1}{i\omega\rho}\nabla p\ . \tag{2}$$

The first quantity in Eq. (1) is the time rate of change of the acoustic energy density, while the second quantity represents the divergence of acoustic intensity, which represents the amount of acoustic energy flowing through a unit of area per unit time.

In practice, the quantity being measured is the real, instantaneous intensity,

$$\vec{J}_i(t)=\mathrm{Re}\left(p(t)\right)\mathrm{Re}\left(\vec{u}(t)\right)\ . \tag{3}$$

Of more general interest, however, is the complex intensity, defined by

$$\vec{J}=\frac{1}{2}p\vec{u}^*\ . \tag{4}$$

Note that one can easily prove that

$$\mathrm{Re}\left(\vec{J}\right)=\frac{1}{T}\int_0^T\vec{J}_i(t)dt=\left\langle\vec{J}_i\right\rangle\ . \tag{5}$$

D'Spain notes[1] that a volumetric array of pressure sensors may be utilized to measure the vector intensity field through estimates of the gradient in Eq. (2). This can be further illustrated by expanding the pressure field in a Taylor series in the vicinity of the observation point, i.e.

$$p\left(\vec{x}\right)\approx p\left(\vec{x}_0\right)+i\omega\rho\left(\vec{x}-\vec{x}_0\right)\bullet\vec{u}\left(\vec{x}_0\right)\ . \tag{6}$$

Thus, complete knowledge of the volumetric pressure field is sufficient to determine the acoustic vector intensity.

A seminal paper on the theoretical foundation of the acoustic vector intensity was provided by Mann, et al.[3] In that work, they showed that a simple description of the pressure field in terms of an amplitude and phase, i.e.

$$p(\vec{r}) = P(\vec{r})e^{i\phi(\vec{r})},\ \vec{u}(\vec{r}) = \frac{e^{i\phi(\vec{r})}}{\omega\rho}\left[P(\vec{r})\nabla\phi(\vec{r}) + i\nabla P(\vec{r})\right], \quad (7)$$

results in the definition of the intensity in terms of a real part and a complex part,

$$\begin{aligned}\vec{J} &= \frac{1}{2\omega\rho}\left[P^2(\vec{r})\nabla\phi(\vec{r}) - iP(\vec{r})\nabla P(\vec{r})\right] \\ &= \vec{I}(\vec{r}) + i\vec{Q}(\vec{r}) \end{aligned} \quad (8)$$

referred to as the active and reactive intensity, respectively. Further, they showed that the reactive part is a physically realizable quantity that cannot be neglected, and is required to properly describe the total acoustic field. They note that "the active intensity is perpendicular to the resultant wave fronts, showing the direction of the resultant wave front propagation," whereas "the reactive intensity … characterizes the spatial pressure magnitude distribution,"[3] as depicted in Fig. 1.

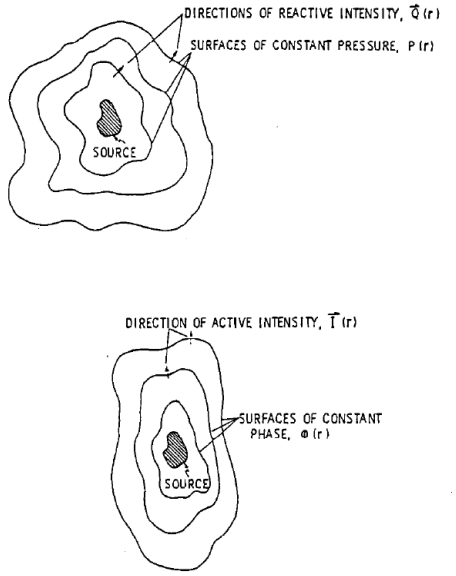

Source: (Mann, et al, 1987)[4]

Figure 1. A general radiated field characterized by surfaces of constant pressure and surfaces of constant phase.

The acoustic vector intensity is the acoustic analog of the Poynting vector in electromagnetic. In part, this motivated Chapman[5] to consider the structure of acoustic intensity streamlines, i.e., those curves whose tangent at every point is parallel to the local average acoustic intensity vector. At any point in space, the tangent to the acoustic intensity streamline may be defined by

$$\phi = \tan^{-1}\left(\langle J_z\rangle / \langle J_r\rangle\right) . \quad (9)$$

Chapman developed a basic iteration scheme to map the streamlines in a simple environment composed of two semi-infinite half-spaces separated by a planar boundary. His results, displayed in Fig. 2, revealed some fundamental differences between the actual flow of acoustic energy and our preconceived views based on ray theory.

Specifically, he noted at low frequency that the acoustic intensity streamlines were barely affected by the presence of the boundary, and energy easily flowed into the lower medium at angles beyond the traditional ray critical angle. At higher frequencies, the streamline behavior below the interface was more consistent with traditional rays, but above the interface the streamline structure became perturbed due to the interference between direct and reflected ray paths.

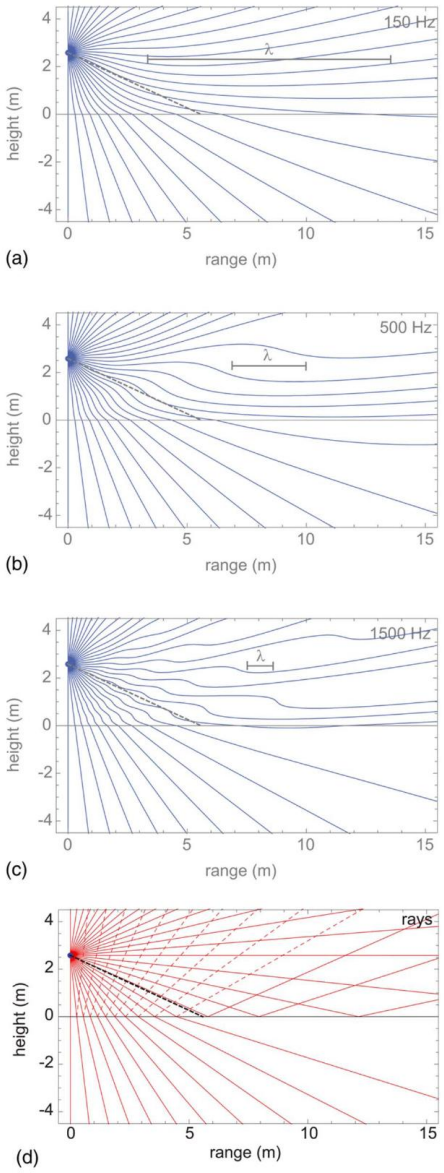

Source: (Chapman, 2008)[6]

Figure 2. Streamlines of energy flow for water-to-sediment transmission: (a) 150 Hz, (b) 500 Hz, (c) 1500 Hz, and (d) the corresponding ray paths. Solid lines: streamline [(a)–(c)] of incident, transmitted, and totally reflected rays (d). Dashed lines: partially reflected rays. Heavy dashed line: critical ray. Associated acoustic wavelengths in water: (a) 10.2 m, (b) 3.1 m, (c) 1.0 m.

Chapman also developed a new plane boundary refraction law for streamlines. Specifically, by noting that both the pressure and vertical velocity components must be continuous across the boundary, then

$$\langle J_{z1}\rangle = \langle J_{z2}\rangle \ . \quad (10)$$

However, the horizontal component of velocity exhibits a discontinuity,

$$\frac{u_{r1}(\theta)}{u_{r2}(\theta)} = \frac{1+R(\theta)}{g^{-1}T(\theta)} = g = \frac{\rho_2}{\rho_1} \quad , \tag{11}$$

and so then does the horizontal component of intensity,

$$\langle J_{r1} \rangle = g \langle J_{r2} \rangle \quad . \tag{12}$$

Therefore, the incident and transmitted angle satisfy a refraction law, illustrated in Fig. 3 and defined by

$$\tan\phi_2 = g \tan\phi_1 \quad . \tag{13}$$

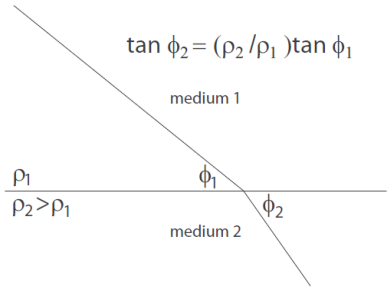

Source: (Chapman, 2008)[7]

Figure 3. Acoustic streamline refraction by a density discontinuity, for the case $\rho_2 > \rho_1$.

SOME VECTOR FIELD PHENOMENOLOGY

Multipath/multisource interference

Many traditional references on acoustic vector sensors assume simple, plane-wave propagation of the field. This leads to a simplified expectation that a single vector sensor can determine direction to a source. While this is true in the presence of single arrivals and/or large signal-to-noise conditions, the influence of multipath, multiple in-band sources, or in-band noise complicates the processing on a single sensor.

In the presence of a plane-wave, the pressure and vector velocity may be defined simply by

$$p = |p| e^{i\vec{k}\bullet\vec{r}} \text{ and } \vec{u} = \frac{|p|}{\rho c}\hat{k} \quad , \tag{14}$$

where $\hat{k} = \frac{\vec{k}}{|\vec{k}|}$ is the direction of propagation. As suggested, the response of a single vector sensor provides enough information to determine the direction of propagation of the field.

In contrast, let us consider another highly simplified view of propagation, specifically the field produced by a single normal mode in an isospeed waveguide. In this environment, the vertical mode structures will be sinusoidal, e.g. $\Psi_M \sim \sin(\gamma_M z)$, where γ_M is the quantized vertical wavenumber component of mode *M*, and will have horizontal phase factors of $e^{iK_M r}$, where K_M is the quantized horizontal wavenumber component. Then

$$\frac{\partial p}{\partial z} \sim \gamma_M \cos(\gamma_M z) \quad , \quad \frac{\partial p}{\partial r} \sim K_M \sin(\gamma_M z) . \tag{15}$$

We note that the resulting ratio of velocity components satisfies

$$\frac{u_z}{u_r} = \frac{\gamma_M}{iK_M} \frac{\cos(\gamma_M z)}{\sin(\gamma_M z)} = -i \frac{\tan\theta_M}{\tan(\gamma_M z)} \quad , \tag{16}$$

which indicates that the velocity field response of a single mode is elliptical in nature. Figure 4 depicts a snapshot of the velocity field in a waveguide with a single mode excited. Averaging of the velocity field would reduce to zero, while an average of the vector acoustic intensity field would reduce to a single, downrange vector indicating the average energy flow down the waveguide. But the direction of the underlying plane waves propagating at $\pm\theta_M$, which create the structure of the mode, is lost in the interference.

Similar vector field complexity would be exist in the presence of multiple sources or a random noise field, assuming the signals occur within the same frequency band. Therefore, in order to uniquely observe angles of interest, coherent processing across an aperture of sensors is still required.

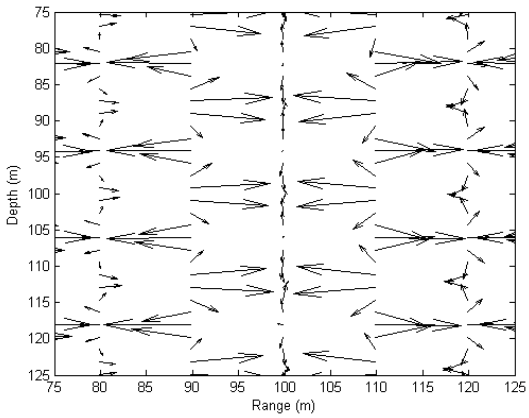

Figure 4. Instantaneous snapshot of velocity vectors in the presence of a single, shallow water normal mode

Plane-wave scattering

Although the complexity of the vector field may complicate extraction of unique information from a single sensor, there are cases where unique features may exist within the field. As an example, consider the near-field structure of acoustic intensity observed by plane-wave scattering from a rigid sphere. The scattered pressure field is known to have the form[8]

$$\boldsymbol{P}_{s\infty}(R,\theta) = -P_i \sum_n (2n+1) i^n P_n(\cos\theta) b_n h_n(kR) , \tag{17}$$

where the $P_n(x)$ refer to the Legendre' polynomials, $j_n(x)$ and $h_n(x)$ refer to spherical Bessel functions, and $b_n = \frac{j_n'(ka)}{h_n'(ka)}$. Although algebraically challenging, the calculation of the associated vector velocity field is reasonably straightforward[9].

By combining the total (incident plus scattered) pressure field wth the total vector velocity field, the structure of the complex intensity field can be determined. Analysis of the radial and angular components of the active and reactive intensity fields reveals a very rich structure that is unique in nature. Figure 5 displays the results of such an analysis for a rigid sphere, radius a, when ensonified by a plane wave satisfying $ka = 3$.

UNDERWATER ACOUSTIC VECTOR FIELD MODELING

In order to be able to study some of the features of the acoustic vector field in underwater acoustic applications, numerical algorithms are desired which are consistent with existing acoustic pressure propagation models. However, the fundamental wave equation for the vector velocity field does not lend itself to direct integration, as the Helmholtz equation for acoustic pressure does. Therefore, methods for computing the velocity field must rely on the solutions to the underlying pressure field and the relationship between the two quantities, defined by Eq. (2). Ideally, such methods should utilize the constructs of the underlying model to ensure the same order of accuracy in the solution.

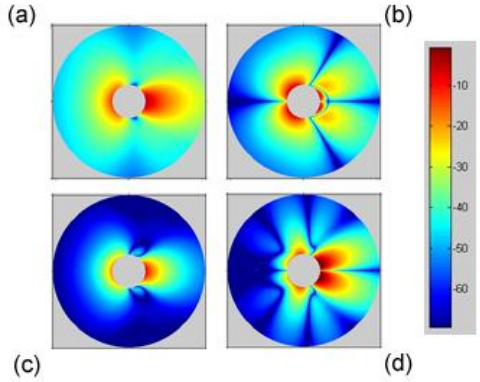

Figure 5. Total field due to plane wave scatter from a rigid sphere ($ka = 3$): (a) radial active, (b) radial reactive, (c) angular active, and (d) angular reactive intensities. Scale of figures is $5a \times 5a$. Colorbar in units of dB.

Parabolic equation methods

The expressions for simultaneous computation of the vector velocity field from implementation of a parabolic equation (PE) model of the underlying pressure field were first defined by Smith, et al.[10] In a straightforward manner, they began by defining the pressure field in terms of the PE field function, $\psi(\vec{r})$, such that

$$p(\vec{r}) = P_0\sqrt{\frac{R_0}{r}}\psi(\vec{r})e^{ik_0 r} \quad , \tag{18}$$

and $\psi(\vec{r})$ is known to satisfy a parabolic equation of the form

$$\frac{\partial\psi}{\partial r} = -ik_0\left(1 - Q_{op}\right)\psi \quad , \tag{19}$$

with operators defined by

$$Q_{op} = \sqrt{1+\mu+\varepsilon}\ , \ \mu = \frac{1}{k_0^2}\frac{\partial^2}{\partial z^2}\ , \text{ and } \varepsilon = n^2 - 1\ . \tag{20}$$

The radial component of the velocity field can then be directly related to the fundamental parabolic equation, which in the far-field takes the form

$$u_r = -\frac{i}{\omega\rho_0}P_0 R_0^{1/2}\left[-\frac{1}{2r^{3/2}} + \frac{ik_0}{r^{1/2}} + \frac{1}{r^{1/2}}\frac{\partial\psi}{\partial r}\right]$$
$$\approx \frac{P_0}{c_0\rho_0}\sqrt{\frac{R_0}{r}}e^{ik_0 r}Q_{op}\psi \quad . \tag{21}$$

Because the solution at any given range step is defined as a vector over depth, the vertical component may be computed by employing a sequence of Fourier transforms, such as

$$u_z = -\frac{iP_0}{\omega\rho_0}\sqrt{\frac{R_0}{r}}e^{ik_0 r}\frac{\partial\psi}{\partial z}$$
$$= \frac{P_0}{c_0\rho_0}\sqrt{\frac{R_0}{r}}e^{ik_0 r}FFT\left[i\frac{k_z}{k_0}IFFT\left(\psi(r,z)\right)\right] \quad . \tag{22}$$

Thus, as Eq. (19) is solved via some iterative scheme (e.g., split-step Fourier, implicit finite difference, finite element, etc.), Eqs. (21) and (22) can be computed locally at each range step. The result is the complete acoustic vector field (pressure and planar components of velocity). Figure 6 displays results of such a calculation for a simple, isospeed, shallow water waveguide.

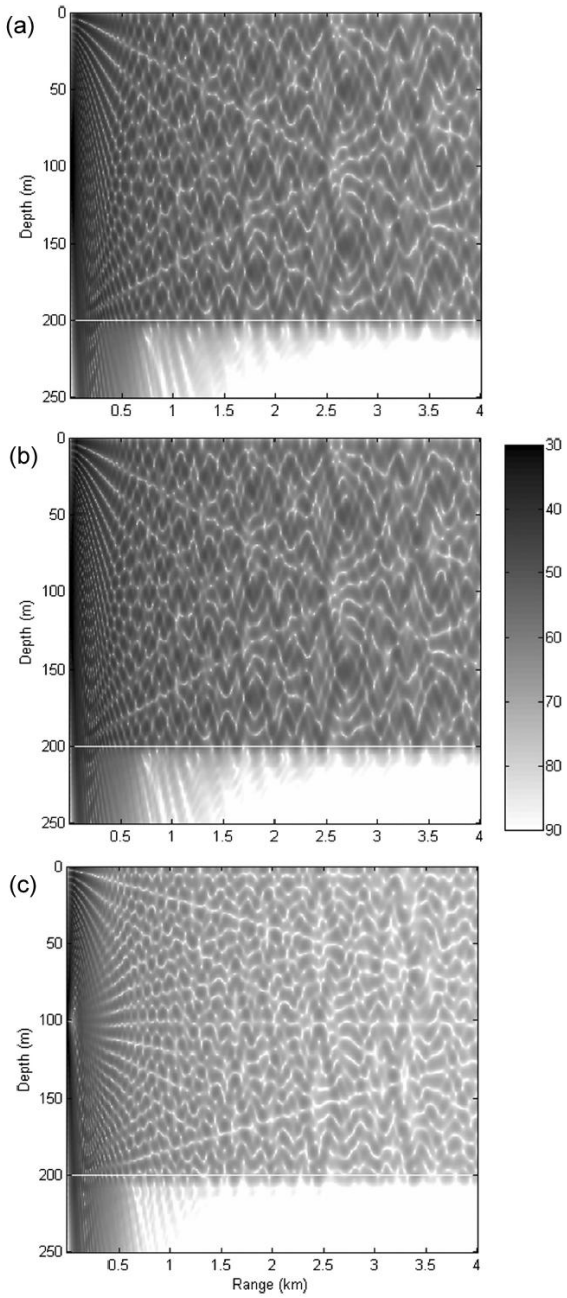

Figure 6. Transmission loss plots (grayscale colorbar units dB re 1m) for a shallow water waveguide: (a) pressure, (b) radial velocity component, and (c) vertical velocity component.

The underlying PE pressure field model had been previously benchmarked, and so the solutions to the vector field should be accurate. It is still desirable, however, to have an independent benchmark of the velocity field results. This can be obtained by evaluating the response for an individual normal mode.

For the purposes of benchmarking, we adapt the expression presented in Eq. (16) to investigate the ratios of the real quantities

$$\frac{\mathrm{Re}(u_z)}{\mathrm{Im}(u_r)} = \frac{1}{K_M}\frac{\partial\Psi_M/\partial z}{\Psi_M} = \frac{\tan\theta_M}{\tan(\gamma_M z)} \quad , \tag{23}$$

and

$$\frac{\mathrm{Re}(u_z)}{\mathrm{Re}(u_r)} = -\frac{\tan\theta_M}{\tan(\gamma_M z)}\cot\left(K_M r - \frac{\pi}{4}\right) \quad . \tag{24}$$

Figure 7 displays the results comparing the output of the MMPE model,[11] updated to compute the velocity field components, with the analytic expressions defined in Eqs. (23) and (24). The solutions are effectively identical, providing excellent confirmation of the accuracy of the numerical method.

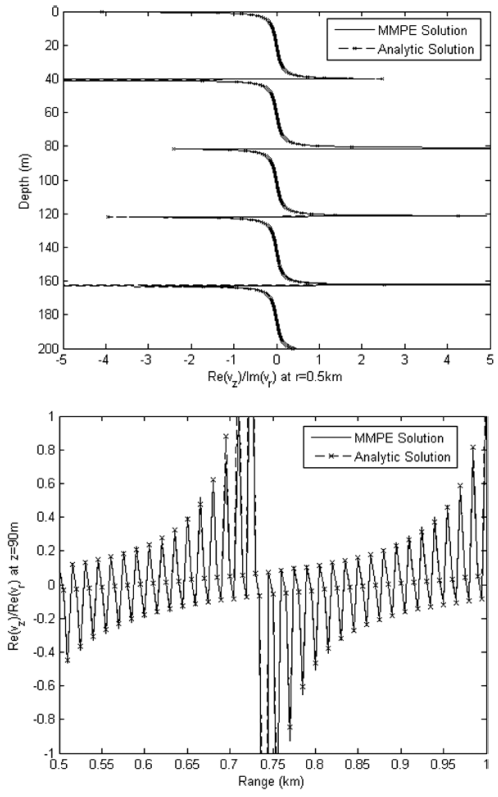

Figure 7. Results from MMPE model for single mode propagation compared with analytic expressions in Eqs. (23) and (24).

Normal mode methods

Pressure field propagation models based on normal mode methods are also very popular. The extension of such models to compute the velocity field has also been shown to be reasonably straightforward.[12] We begin by stating the local range description (i.e., in the j^{th} range step) of the pressure field in terms of the local normal modes, $\Psi_m^{(j)}(z)$,[13]

$$p^{(j)}(r,z) = P_0\sum_{m=1}^{M}\left[a_m^{(j)}H1_m^{(j)}(r) + b_m^{(j)}H2_m^{(j)}(r)\right]\Psi_m^{(j)}(z), \tag{25}$$

where the factors $a_m^{(j)}$ and $b_m^{(j)}$ define the local amplitudes of the outgoing and incoming modes, and

$$H1_m^{(j)}(r) = \sqrt{\frac{r_{j-1}}{r}}e^{iK_m^{(j)}(r-r_{j-1})}\ ,\ H2_m^{(j)}(r) = \sqrt{\frac{r_{j-1}}{r}}e^{-iK_m^{(j)}(r-r_{j-1})}. \tag{26}$$

Range-dependent solutions are generated by computing mode coupling coefficients[13] that define the amount of modal energy transfer between range steps,

$$\tilde{c}_{nm}^{(j)} = \int\frac{\Psi_n^{(j+1)}(z)\Psi_m^{(j)}(z)}{\rho^{(j+1)}(z)}dz \ , \text{ and}$$
$$\hat{c}_{nm}^{(j)} = \frac{K_m^{(j)}}{K_n^{(j+1)}}\int\frac{\Psi_n^{(j+1)}(z)\Psi_m^{(j)}(z)}{\rho^{(j)}(z)}dz \ . \tag{27}$$

The corresponding expressions for the radial and vertical velocity components are then simply

$$u_r^{(j)}(r,z) = -\frac{i}{k^{(j)}(r,z)}\frac{P_0}{\rho^{(j)}c^{(j)}(r,z)}\times$$
$$\sum_{m=1}^{M}K_m^{(j)}\left[a_m^{(j)}H1_m^{(j)}(r) - b_m^{(j)}H2_m^{(j)}(r)\right]\Psi_m^{(j)}(z), \tag{28}$$

and

$$u_z^{(j)}(r,z) = -\frac{i}{k^{(j)}(r,z)}\frac{P_0}{\rho^{(j)}c^{(j)}(r,z)}\times$$
$$\sum_{m=1}^{M}\left[a_m^{(j)}H1_m^{(j)}(r) + b_m^{(j)}H2_m^{(j)}(r)\right]\frac{d\Psi_m^{(j)}}{dz}(z) \ . \tag{29}$$

Note that Eqs. (28) and (29) can be computed directly with the existing solutions of the normal modes and corresponding modal wavenumbers. The only additional calculation required is the vertical derivative of the normal mode. The horizontal and vertical boundary conditions of the velocity components are already satisfied by the coupling coefficients.

The Couple97 normal mode model[14] was updated to incorporate Eqs. (28) and (29). The evaluation of the vertical derivative was trivial since the mode shapes were computed using the Galerkin method which utilizes a summation over sinusoids. Sample results of this model output compared against an analytic solution for a simple, shallow water waveguide are displayed in Fig. 8. Again, the quality of the agreement is indicative of the accuracy of the numerical implementation.

APPLICATIONS OF VECTOR FIELD PROCESSING

As stated previously, early work in vector field processing studied the directionality of the low-frequency noise field. With the introduction of more and better sensors, many in the underwater acoustics research community are exploring the use of such data for other applications.

Ocean seafloor inversions

One area that receives a considerable amount of attention is environmental inversions based on acoustic data collected from sea trials. This includes the field of geo-acoustic inversions, whereby acoustic data is used to infer information about the seafloor sediment and substrata. A large number of inversion algorithms have been developed based on minimization of a cost function through some optimized search rou-

tine, such as simulated annealing or genetic algorithms.[e.g., 15, 16]

The introduction of the acoustic vector data into these inversion algorithms has recently been achieved by several investigators.[e.g., 17, 18, 19] The results seem to suggest that the number of iterations required to find a suitable solution is reduced when the additional information in the vector field is included. What remains unclear, however, is whether the additional information actually increases the accuracy (or reduces the variance) of the solution. Part of the issue may be that these approaches rely on the same general cost function minimization techniques, rather than attempt to utilize unique features of the vector field.

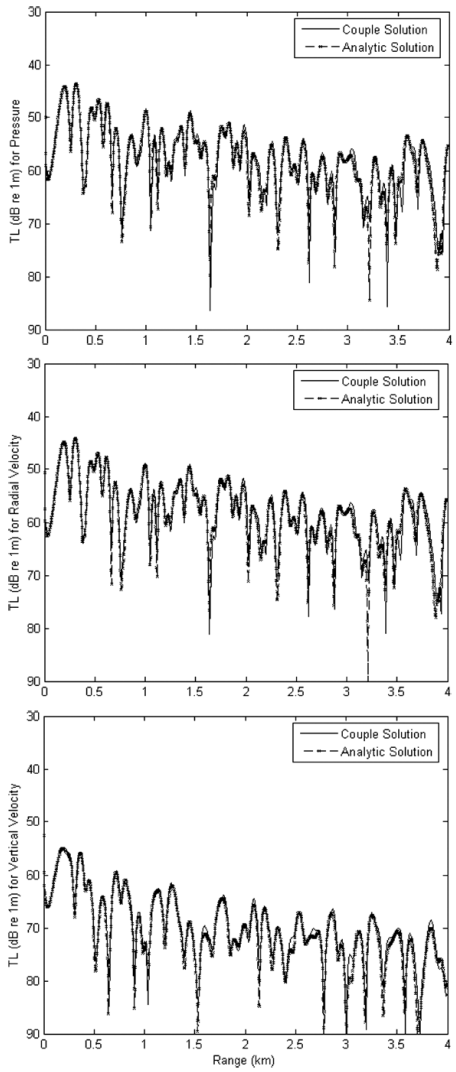

Figure 8. Results from Couple97 normal mode model compared with analytic model for simple waveguide.

To this end, Smith, et al.[20] showed that measurements of the modal vector intensity field could be exploited to make direct estimates of modal attenuation. This information could be inverted to provide profiles of bottom attenuation, a parameter known to exhibit large variability in standard inversion algorithms. The estimates are based on determining the active and reactive components of the complex vector intensity for a single mode. When attenuation is present, it can be shown[20] that these quantities have the form

$$\vec{I} = \frac{\omega\rho}{2r}\left|A_M\right|^2\left|\Psi_M(z)\right|^2 e^{-2\delta_M r}\hat{r} \ , \qquad (30)$$

and

$$\vec{Q} = -\frac{\omega\rho\left[\delta_M + \frac{1}{2r}\right]}{2K_M r}\left|A_M\right|^2\left|\Psi_M(z)\right|^2 e^{-2\delta_M r}\hat{r} + \frac{\omega\rho}{2K_M r}\left|A_M\right|^2\Psi_M(z)\frac{d\Psi_M(z)}{dz}e^{-2\delta_M r}\hat{z} \ , \qquad (31)$$

where $\Psi_M(z)$ are the mode functions of amplitude A_M, and the modal attenuation factor is δ_M. It can then be observed that the ratio between the radial components of the reactive and active intensities asymptotically provides an estimate of the modal attenuation factor,

$$\left|\frac{Q_r}{I_r}\right| = \frac{\left[\delta_M + \frac{1}{2r}\right]}{K_M} \approx \frac{\delta_M}{K_M} \ . \qquad (32)$$

Figure 9 displays an example of the asymptotic behaviour of this ratio from an analytic solution. The ratio response of three different modes is presented to illustrate the advantage of evaluating the higher order modes. While such an analysis based on real data is understandably more challenging, this approach does suggest opportunities to extract additional information directly from the vector intensity field.

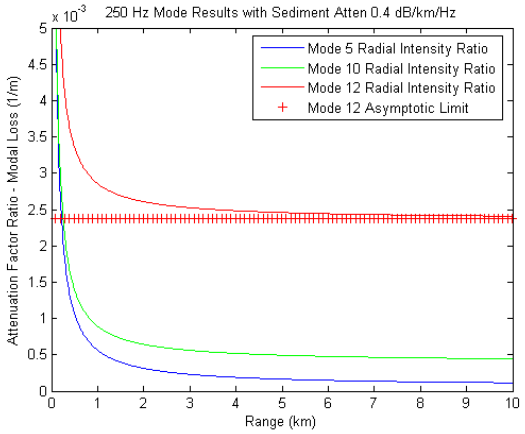

Figure 9. Sample calculation of asymptotic evaluation of modal attenuation factor from ratio of reactive to active radial intensity components.

Line array beamforming

The majority of work involving signal processing of underwater acoustic vector sensor data has been devoted to processing of a linear array of sensors. Studies comparing processing gains from the calculation of array intensity versus combinations of vector components have shown that the latter methods are generally superior.[21]

The most basic form of vector component combination processing is simple linear processing, whereby the components are weighted and summed together. The underlying motivation for this is the observation that the vector velocity sensor has a dipole response, half of which is in phase with the pressure and half of which is out of phase. By simply summing the various components with the pressure, a cardiod response is achieved on each sensor. The inherent directionality of each sensor then increases the overall directionality of the array.

Specifically, linear processing of an array of vector sensors produces a beam response when steered in the solid angle direction $\Theta_s = (\theta_s, \phi_s)$ defined by

$$B^{(pu)}(\theta_s,\phi_s) = \left|\sum_n \left(w_{xn}u_{xn} + w_{yn}u_{yn} + w_{zn}u_{zn} + w_{pn}u_{pn}\right)e^{-i\vec{k}_s\bullet\vec{r}_n}\right|^2, \quad (33)$$

where the velocity components (including a rescaled pressure measurement) are defined by

$$\vec{u}_n = \vec{U}_n e^{i\vec{k}\bullet\vec{r}_n} \text{ (e.g., } u_x = U_x e^{i\vec{k}\bullet\vec{r}_n}\text{), } u_{pn} = \frac{P_n}{\rho c}e^{i\vec{k}\bullet\vec{r}_n} \ . \quad (34)$$

The coherent array processing is achieved by steering the array phase according to $\vec{k}_s\bullet\vec{r}_n = kz_n\cos\theta_s$, while the individual sensors are steered by using weights defined by

$$w_{xn} = Aw_n\cos\theta_s, \ w_{yn} = Bw_n\sin\theta_s\cos\phi_s, \ w_{zn} = Cw_n\sin\theta_s\sin\phi_s, \text{ and } w_{pn} = w_n \ . \quad (35)$$

Note that we assume here the individual vector sensors are being steered in directions consistent with the array phase, i.e. $\Theta_s = (\theta_s,\phi_s)$. In general, however, each sensor could be steered independently of one another.

When the weighting variables $A = B = C = 1$ in (35), each sensor produces the cardiod pattern. For a plane-wave arriving broadside, an array of such sensor patterns produces the array response depicted in Fig. 10. The upper pattern displays the result when pressure-only sensors are employed, and the lower pattern displays the result of utilizing vector sensors. Cray and Nuttall[22] showed that, in addition to the reduction of the right/left ambiguity effect, an array of vector sensors may also provide an optimal performance gain of approximately 5 dB.

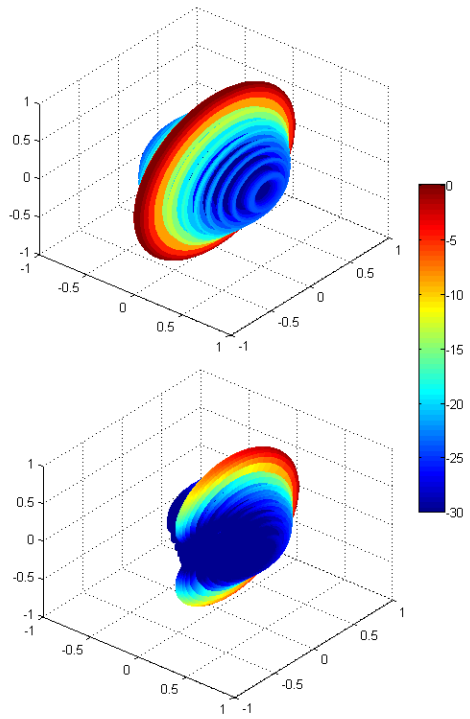

Figure 10. Line array response to broadside arrival using linear beamforming: (upper) pressure-only sensors; (lower) vector sensors steered using basic cardioids.

By changing the relative values of the weighting variables, directional nulls can be steered in various directions. Other, non-linear combinations of weighting variables have been employed to increase the directivity of individual sensors.[23] The advantages of some of these techniques is still unclear, however.

Still others are investigating methods of non-linear, adaptive processing for arrays of vector sensors. These promise to provide the most gain and best directionality.

SUMMARY

In this paper, the fundamentals of the vector acoustic intensity field have been described. Phenomenology that is sometimes counter-intuitive has also been presented that requires us to reconsider some of our preconceived notions of energy flow in the acoustic field. Unique structures in the field and relationships between intensity components have also suggested that the vector field may provide additional insight into the underlying physics of the propagation.

Numerical methods for computing the acoustic velocity field in ocean acoustic waveguides were also presented. These techniques were shown to be reasonably straightforward extensions of existing models for pressure field propagation. Additionally, some analytical expressions were defined that can be used to benchmark updated codes.

Although the general principles of acoustic energy flow have been understand for many years, the formal description of vector acoustic intensity in terms of active and reactive intensities was developed relatively recently. Today, an understanding of the phenomenology associated with the vector field in complex, underwater environments is motivating a growing number of basic and applied research programs. This, along with the introduction of new, sophisticated sensors capable of determining the vector velocity field, is leading to new applications in undersea studies.

REFERENCES

1. G. L. D'Spain, W. S. Hodgkiss, and G. L. Edmonds, "Energetics of the deep ocean's infrasonic sound field," *J. Acoust. Soc. Am.* **89**, 1134-1158 (1991).
2. G. L. D'Spain, W. S. Hodgkiss, and G. L. Edmonds, "The simultaneous measurement of infrasonic acoustic particle velocity and acoustic pressure in the ocean by freely drifting Swallow floats," *IEEE J. Oceanic Eng.* **16**, 195-207 (1991).
3. J. A. Mann, J. Tichy, and A. J. Romano, "Instantaneous and time-averaged energy transfer in acoustic fields," *J. Acoust. Soc. Am.* **82**, 17-29 (1987).
4. Reprinted with permission from [J. A. Mann, J. Tichy, and A. J. Romano, "Instantaneous and time-averaged energy transfer in acoustic fields," *J. Acoust. Soc. Am.* **82**, pg. 19 (1987)]. Copyright [1987], Acoustical Society of America.
5. D.M.F. Chapman, "Using streamlines to visualize acoustic energy flow across boundaries," *J. Acoust. Soc. Am.* **124**, 48-56 (2008).
6. Reprinted with permission from [D.M.F. Chapman, "Using streamlines to visualize acoustic energy flow across boundaries," *J. Acoust. Soc. Am.* **124**, pg. 52 (2008)]. Copyright [2008], Acoustical Society of America.
7. Reprinted with permission from [D.M.F. Chapman, "Using streamlines to visualize acoustic energy flow across boundaries," *J. Acoust. Soc. Am.* **124**, pg. 55 (2008)]. Copyright [2008], Acoustical Society of America.
8. F.M. Junger and D. Feit, *Sound, Structures, and Their Interactions* (Acoust. Soc. Am., New York, 1993) Chap 10.
9. R. Barton and K.B. Smith, "Characterization of the near scattered acoustic vector field," *J. Acoust. Soc. Am.* **124**, 2583 (2008).

10. K.B. Smith, G.D. D'Spain, and W.S. Hodgkiss, "Modeling acoustic particle velocity in range dependent environments with a parabolic equation code," *J. Acoust. Soc. Am.* **94**, 1885 (1993).
11. K.B. Smith, "Convergence, stability, and variability of shallow water acoustic predictions using a split-step Fourier parabolic equation model," *J. Comp. Acoust.* **9**, 243-285 (2001).
12. K.B. Smith, "Validating range-dependent, full-field models of the acoustic vector field in shallow water environments," J. Comp. Acoust., Vol. 16, 471-486, 2008.
13. F.B. Jensen, W.A. Kuperman, M.B. Porter, and H. Schmidt, *Computational Ocean Acoustics* (American Institute of Physics, New York, 1994), pp. 299-301.
14. R.B. Evans, "A coupled mode solution for acoustic propagation in a waveguide with stepwise depth variations of a penetrable bottom," *J. Acoust. Soc. Am.* **74** 188–195 (1983).
15. P. Gerstoft, "Inversion of seismoacoustic data using genetic algorithms and a posteriori probability distributions," *J. Acoust. Soc. Am.* **95**, 770-782 (1994).
16. S.E. Dosso, "Quantifying uncertainty in geoacoustic inversion. I. A fast Gibbs sampler approach," *J. Acoust. Soc. Am.* **111**, 129-142 (2002).
17. M. Berrada, M. Meyer, M. Asch, J.-P. Hermand, and K.B. Smith, "Efficient semi-automatic adjoint generation and its application for implementing acoustic particle velocity in geoacoustic inversion," *Proc. 8th Intl. Conf. Theor. and Comp. Acoust.*, 2-5 July 2007, Crete, Greece.
18. S.E. Crocker, J.H. Miller, K.B. Smith, P.C. Hines, and J.C. Osler, "Geoacoustic inversion using specific acoustic impedance," *J. Acoust. Soc. Am.* **126**, 2234 (2009).
19. A.V. van Leijen, *The Sound of Sediments: Acoustic Sensing in Uncertain Environments* (Ph.D. Dissertation, University of Amsterdam, 2010.
20. K.B. Smith, J.-P. Hermand, and A.V. van Leijen, "Estimation of sediment attenuation from measurements of the acoustic vector field," *Proc. 8th Intl. Conf. Theor. and Comp. Acoust*., 2-5 July 2007, Crete, Greece.
21. P.C. Hines, D.L. Hutt, B. Maranda, and V.W. Young, "Comparison of superdirective array and intensity array processing," *Proc. 7th Intl. Cong. Sound and Vibr*., 4-7 July 2000, Garmisch Partenkirken, Germany.
22. B.A. Cray and A.H. Nuttall, "Directivity factors for linear arrays of velocity sensors," *J. Acoust. Soc. Am.* **110**, 324-331 (2001).
23. K.B. Smith, and A.V. van Leijen, "Steering vector sensor array elements with cardioids, hippopedes, and other beam shapes," *J. Acoust. Soc. Am.* **122**, 370-377 (2007).